Supplementary Material

Dinuclear vs Tetranuclear $Co^{II}Y^{III}$ complexes: The effect of increasing molecular size on the relaxation dynamics.

Alberto Masegosa, M. Palacios, Eliseo Ruiz, Silvia Gómez-Coca, J. Krzystek, José. M. Moreno, Enrique Colacio

Table S1. Crystallographic data for $[\{Co(\mu\text{-}L)Y(NO_3)\}_2(\mu\text{-}CO_3)_2]\cdot 2CH_3OH\cdot 2H_2O$ **(1)**.

Formula	$C_{54}H_{86}N_8O_{24}Co_2Y_2$
Mw	1526.98
Crystal system	Monoclinic
Space group (no.)	P21/n (14)
a (Å)	12.959(3)
b (Å)	12.394(3)
c (Å)	19.345(4)
α (°)	90.000(3)
β (°)	94.40(3)
γ (°)	90.000(3)
V (Å^3)	3097.9(11)
Z	2
Dc (g cm^{-1})	1.637
μ(MoK$_\alpha$) (mm^{-1})	2.468
T (K)	100(2)
Observed reflections [a]	6376 (5534)
Rint	0.0536 (0.0290)
Parameters	433
GOF	1.117
R1 [b]	0.0413 (0.0305)
wR^2 [c]	0.0749 (0.0695)
Largest peak and hole (e Å^{-3})	0.432 and -0.866
[a] Values in parentheses for reflections with I > 2σ(I). [b] R1 = Σ||Fo| - |Fc||/Σ|Fo|. [c] wR2 = {Σ[w(Fo² - Fc²)²] / Σ[w(Fo²)²]}½.	

Table S2. Selected distances and angles for $[\{Co(\mu\text{-}L)Y(NO_3)\}_2(\mu\text{-}CO_3)_2]\cdot 2CH_3OH\cdot 2H_2O$ **(1)**.

Bond	amstrongs	Bond/distance	armstrongs
Co2- N1	2.182(2)	Y1-O5	2.3607(17)
Co2-N2	2.199(2)	Y1-O5 (I)	2.3530(17)
Co2-N3	2.250(2)	Y1-O7	2.3886(17)
Co2-O2	2.1542(17)	Y1-O9	2.5818(18)
Co2-O3	2.0998(18)	Y1-O10	2.4613(18)
Co2-O6	2.0708(17)	Y1···Co2	3.4873(7)
Y1-N7	2.955(2)	Co2···Co2 (I)	8.278(2)

Y1-O2	2.2939(17)	Y1···Y1 (I)	3.9987(10)
Y1-O3	2.2833(17)	Co2···Co2 (II)	8.290(2)
Y1-O4	2.5328(19)	Co2···Co2 (III)	8.4321(15)
I= 1-x, 1-y, -z; II= -x, 1-y, -z; III= ½-x, -½+y, ½-z or ½-x, ½+y, ½-z			
Angle	**degrees**	**Angle**	**degrees**
N1-Co2-N2	80.44(8)	O3-Co2-N3	90.18(8)
N1-Co2-N3	102.10(8)	O3-Co2-O2	77.37(7)
N2-Co2-N3	80.42(8)	O6-Co2-N1	96.18(8)
O2-Co2-N1	90.04(7)	O6-Co2-N2	167.60(7)
O2-Co2-N2	98.20(7)	O6-Co2-N3	88.70(8)
O2-Co2-N3	167.31(7)	O6-Co2-O2	93.72(7)
O3-Co2-N1	166.25(7)	O6-Co2-O3	90.17(7)
O3-Co2-N2	95.76(8)		

Table S3.- Continuous Shape Measures calculation for the CoN_3O_3 coordination polyhedron of **1**.

```
-------------------------------------------------------------------------------
S H A P E   v2.1         Continuous Shape Measures calculation
(c) 2013  Electronic Structure Group, Universitat de Barcelona
                Contact:  llunell@ub.edu
-------------------------------------------------------------------------------

JPPY-6         5 C5v   Johnson pentagonal pyramid J2
TPR-6          4 D3h   Trigonal prism
OC-6           3 Oh    Octahedron
PPY-6          2 C5v   Pentagonal pyramid
HP-6           1 D6h   Hexagon

Structure [ML6 ]      JPPY-6      TPR-6       OC-6       PPY-6       HP-6
        ,              25.478,     11.801,     1.444,     22.035,     30.762
```

Table S4.- Contributions to *D*-tensor from CASSCF QDPT calculations.

Compound	**1**	
	D	*E*
$^4\Phi_1$	52.477	-52.062
$^4\Phi_2$	31.225	-30.306
$^4\Phi_3$	-2.333	0.813
$^4\Phi_4$	-6.439	1.340
$^4\Phi_5$	-4.410	1.342

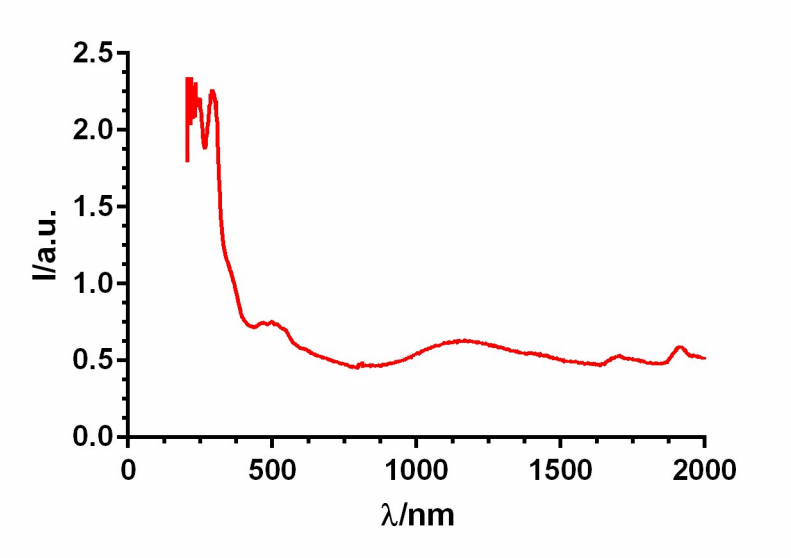

Figure S1 .- UV-vis-NIR solid state reflectance spectra for **1**.

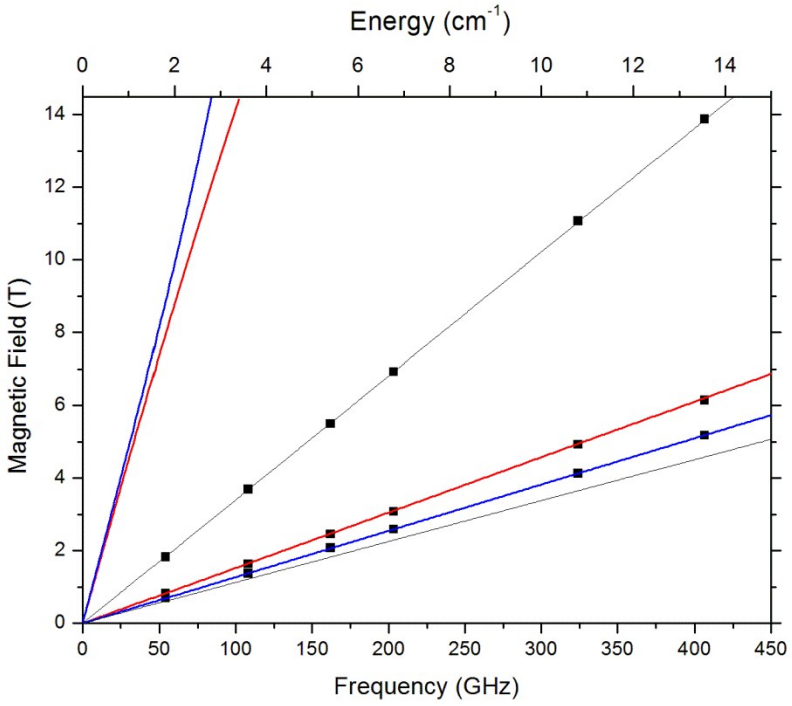

Figure S2. Field vs. frequency (or energy) dependence of the turning points in the powder spectra of **1** at 5 K. The squares represent experimental resonances while the lines were drawn using the same spin Hamiltonian parameters as in caption to Figure 3. Red lines: turning points with magnetic field parallel to the *x*-axis of the zero-field splitting tensor; blue lines: B_0 || *y*; black lines: B_0 || *z*. The lines that have no squares on them represent

turning points of the intra-Kramers transition within the m_s= ±3/2 doublet, which is not populated at low temperature, as *D* is large, and positive.

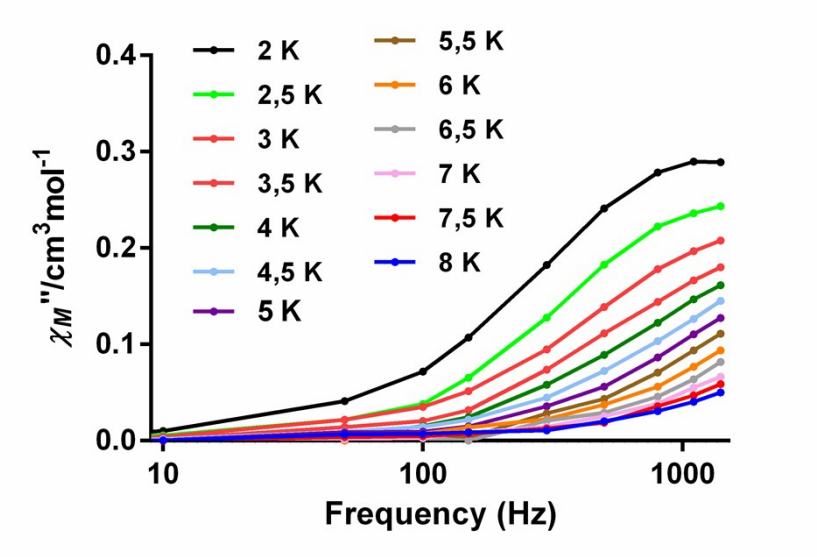

Figure S3.- Frequency dependence of the out-of-phase ac susceptibility for **1** under a magnetic field of 0.025 T at different temperatures.

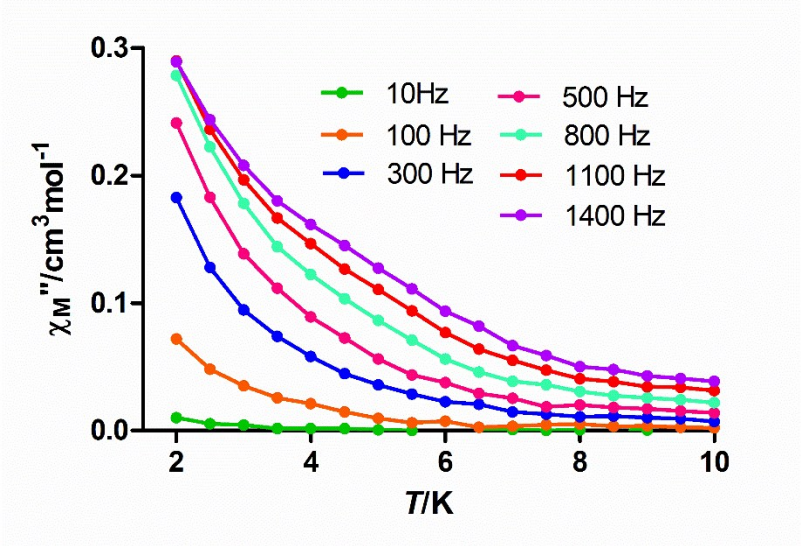

Figure S4.- Temperature dependence of the out-of-phase ac susceptibility for **1** under a magnetic field of 0.025 T at different frequencies.

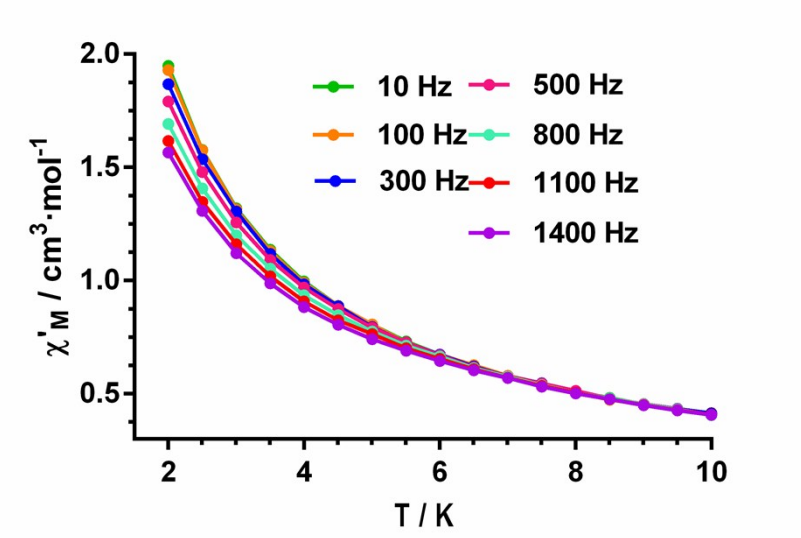

Figure S5.- Temperature dependence of the in-phase ac susceptibility for **1** under a magnetic field of 0.025 T at different frequencies.

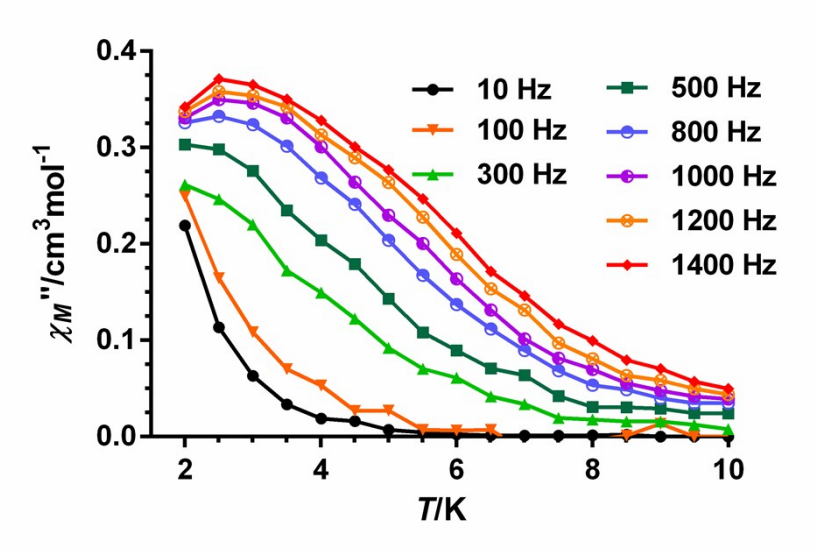

Figure S6.- Temperature dependence of the out-of-phase ac susceptibility for **1** under a magnetic field of 0.2 T at different frequencies.

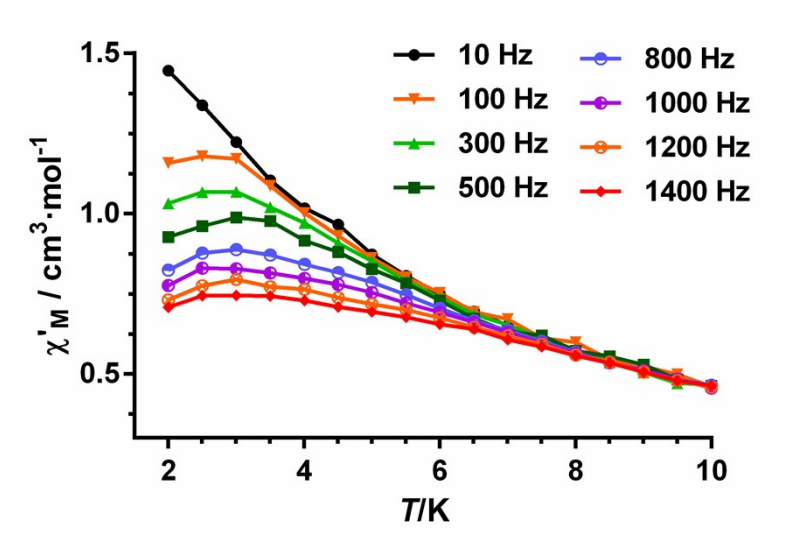

Figure S7.- Temperature dependence of the in-phase ac susceptibility for **1** under a magnetic field of 0.2 T at different frequencies.

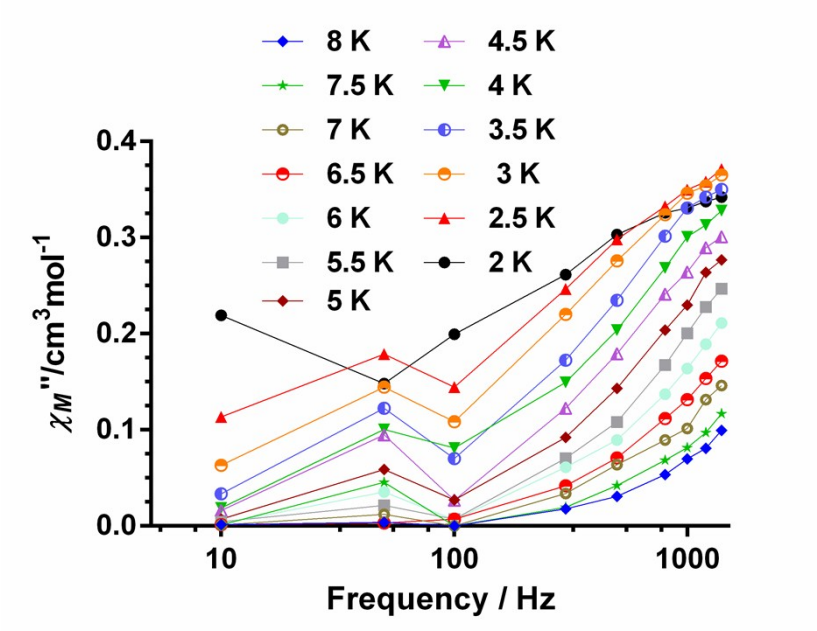

Figure S8.- Frequency dependence of the out-of-phase ac susceptibility for **1** under a magnetic field of 0.20 T at different temperatures

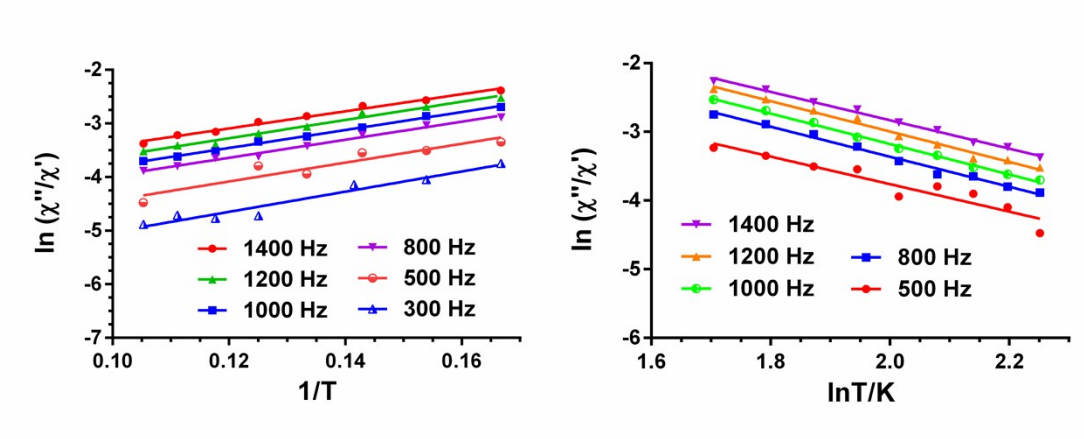

Figure S9.- Temperature dependence of the ratio of the in-phase and out-of-phase *ac* components at different frequencies under a magnetic field of 0.2 T for **1**. Solid lines correspond to the fit of the experimental data to equation 4 (left) and equation 5 (right).

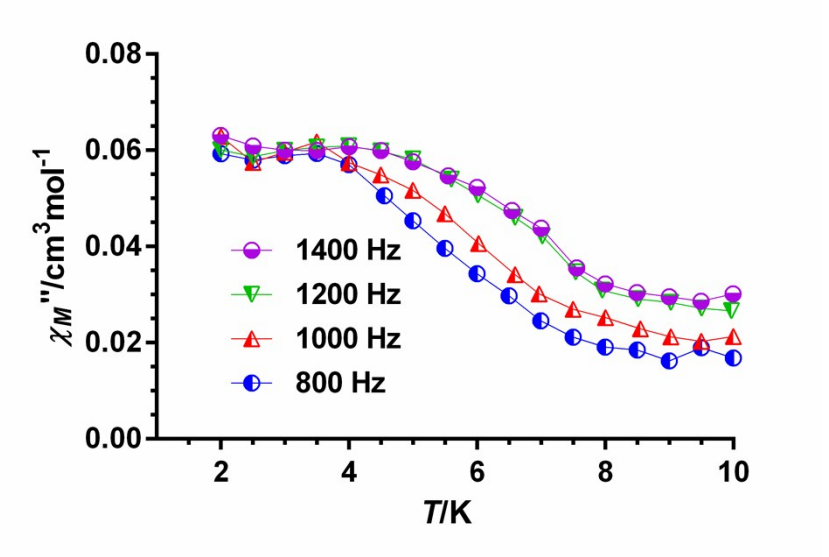

Figure S10.- Temperature dependence of the out-of-phase ac susceptibility for **1'** under a magnetic field of 0.20 T at different frequencies.

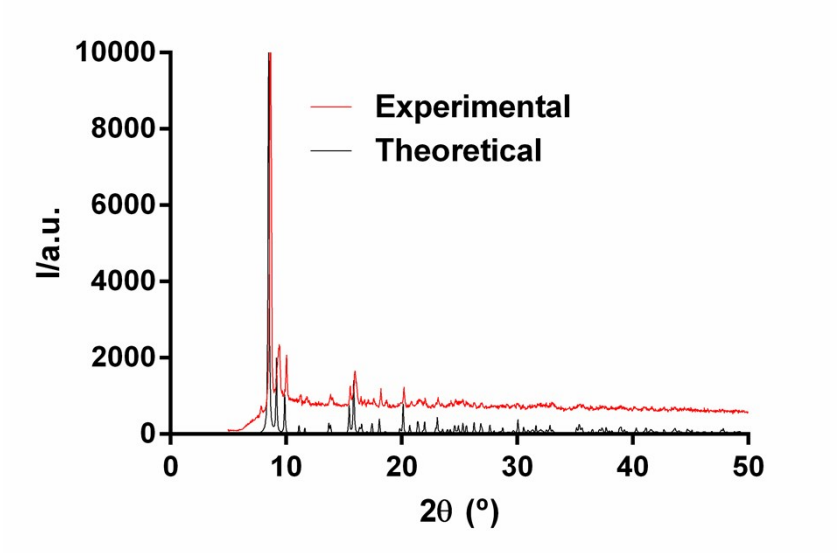

Figure S11.- Experimental and calculated Powder X-Ray diffraction diagrams for **1'**.